Focal Mechanisms from Waveform Inversion and Multiple Velocity Models: Phayao Fault Zone, Northern Thailand

Kasemsak Saetang[1] and Helmut Duerrast[1*]

Abstract

Northern Thailand, situated within the complex Sunda Tectonic Plate, shows significant seismic activity due to its proximity to major tectonic boundaries; however, it often has lower to medium magnitudes. One of the delineated active fault zones is the Phayao Fault Zone (PFZ), which generated an M_w 6.3 earthquake in 2014. Its further south located Pan Segment is also active, but with lower magnitudes. However, understanding and characterizing its seismicity is essential for ongoing seismic hazard assessment of the area. To overcome the challenges, waveform inversion techniques in combination with multiple velocity models were employed, with the aim to characterize the seismic source parameters of earthquakes in this area. Hypocentres were determined with exceptional precision and subsequently validated by applying a velocity model that demonstrated the highest double-couple percentage. This indicates the model's efficacy in precisely calculating hypocentral parameters in this specific geological context. Our findings unveil a complex interplay between right-lateral strike-slip and reverse faulting mechanisms, consistent with a transpressional tectonic regime in the Pan Segment. This regime reflects the accommodation of regional compressional stresses superimposed on the dominant strike-slip motion along the Phayao Fault Zone, thereby yielding a significant contribution to seismic hazard assessment in Northern Thailand. The study also underscores the need for further research to refine these models and methodologies, thereby enhancing our understanding of the seismic characteristics of earthquakes in such regions. Methodologies and insights gained here could serve as a model for characterizing seismic source parameters in other understudied low-seismicity regions globally.

Keywords: Focal mechanism, ISOLA, Velocity model, Waveform inversion, Hypocenter determination

[1] Division of Physical Science, Faculty of Science, Prince of Songkla University

[*] Corresponding author e-mail: helmut.j@psu.ac.th

DOI: https://doi.org/10.65217/wichchajnstru.2026.v45i1.267341

Received: 24 April 2025, Revised: 2 May 2025, Accepted: 6 May 2025

Introduction

Located within the Sunda tectonic plate in Southeast Asia, Thailand demonstrates considerable seismic activity, as shown in Figure 1, which is partly attributed to the country's proximity to the Sunda Subduction Zone, a component of the globally recognized 'Ring of Fire', and partly related to active faults, which are the result of the India-Eurasian continent-continent collision. The latter ones are responsible for the seismicity in Thailand's western and northern regions. In terms of its tectonic setting, Thailand lies between the Shan-Thai Terrane (STT) to the west and the Indochina Terrane (ICT) to the east (Aihara *et al*., 2007). During the uplift of the Himalayas during the Cenozoic era, Thailand experienced tectonic and geologic events that resulted in the development of diverse geological structures, as outlined by Morley *et al*. (2011), including the formation of the Khorat Plateau in northeastern Thailand. Additionally, regions such as the Andaman Sea (AS), Central Basin (CB), Gulf of Thailand (GOF), Peninsular Thailand (PT), and Western Thailand (WT) have also been influenced by these tectonic processes, leading to the creation of a variety of geological features, including active faults, and sedimentary deposits in extensional basin structures (Figure 1). A comprehensive understanding of these Cenozoic processes is crucial for unraveling the geological framework and evolutionary history of Thailand and its surrounding marine regions as it carries significant implications for geological hazards and natural resources, including substantial reserves of hydrocarbon and lignite, as well as mineral deposits (Morley *et al*., 2011).

The structural geology of Thailand during the Cenozoic era is characterized by a combination of compression, strike-slip faulting, and folding, all of which can be attributed to the tectonic stresses within the region as a result of the Indian-Eurasian continent-continent collision (Morley *et al*., 2011). Northern Thailand is characterized by mountain ranges and Tertiary basins formed by extensional escape tectonics (Uttamo, 2000). A variety of rock types can be found in the basins alongside younger sedimentary rocks (Department of Mineral Resources (DMR), 2007).

Regarding the seismicity of Thailand and surrounding areas, notable earthquakes include the M_w 9.2 Sumatra-Andaman earthquake on December 26, 2004, which caused significant damage, tsunamis, and loss of lives across the country and the region. Further, a 6.3 magnitude earthquake occurred on May 5, 2014, located at the Phayao Fault Zone (PFZ), resulting in one fatality. However, after the M_w 9.2 event, the Thai Meteorological Department (TMD) significantly improved Thailand's seismic monitoring network by increasing the number of seismic stations. These improvements have resulted in enhanced earthquake detection, more accurate location determination, ground-motion assessment, and a more comprehensive seismic hazard evaluation (Thai Meteorological

Department (TMD), 2014) TMD is the sole government agency responsible for continuous earthquake monitoring and reporting; however, the resulting data are frequently used for academic research (Noisagool *et al*., 2014; Saetang and Duerrast, 2023).

Seismological research in Thailand has significantly increased following the M_w 9.2 Sumatra-Andaman earthquake, leading to a better understanding of Thailand's seismicity and seismic hazard. Noisagool *et al*. (2014) conducted a study investigating crustal thicknesses across Thailand, ranging from 28 to 42 km. Saetang (2022) published research work done on mantle anisotropy, presenting a two-layer model and concluding that the movement within the Shan-Thai Terrane is more complex than that within the West-Burma Terrane. Furthermore, Saetang *et al*. (2018) presented local earthquake tomography to explore geothermal sources and pathways beneath the crust of Northern Thailand. Recently, Saetang and Duerrast (2023) published a 1-D velocity model with station delays for northern Thailand, demonstrating significantly lower root-mean-square values of travel time residuals. They also demonstrated a clear relationship between station delays and near-surface geology. However, an understanding of Thailand's complex tectonic details is still required. While previous focal mechanism studies (Noisagool *et al*., 2014; Pananont *et al*., 2017; Saetang, 2017) concentrated on the Mae Lao Segment following the 2014 M_w 6.3 earthquake, the Pan Segment has remained largely uncharacterized in terms of its seismic source parameters. The 2019 earthquake sequence provides an opportunity to constrain the faulting style and tectonic regime of this southern segment, thereby extending our understanding of strain partitioning along the entire Phayao Fault Zone. Although seismic activity in Thailand is generally lower compared to surrounding countries such as Myanmar, it remains susceptible to earthquakes due to its proximity to major fault zones (see Figure 1 and 2). Several geological areas exhibit a relatively higher degree of seismicity, particularly in the northern and western regions adjacent to Myanmar and Laos.

This investigation is focusing on the Phayao Fault Zone (PFZ), which is divided into the Mae Lao Segment (MLS) in the north and the Pan Segment (PS) in the south, as delineated in Figure 2 (Boonchaisuk *et al*., 2017), and which generated the M_w 6.3 earthquake on 5 May 2014 in its northern section. Subsequent studies by Noisagool *et al*. (2014), Pananont *et al*. (2017), and Saetang (2017) used moment tensor solutions to estimate the geometry of this northern segment. They revealed main shock magnitudes between M_w 6.2 and M_w 6.5 and aftershock depths ranging from 10 to 15 km. The present study, however, is focusing on the Pan Segment in the southern part of the PFZ. The central question of this research is how waveform inversion techniques and multiple velocity models, including the recently developed Saetang and Duerrast (2023) model, can be effectively employed to characterize the seismic source parameters of

earthquakes in this specific region, ultimately improving seismic hazard assessment for Northern Thailand. In pursuit of this, we aim to determine the focal mechanism of the M_w 4.9 earthquake reported by the Thai Meteorological Department (TMD) in February 2019. Moreover, the methodologies and insights gained here could serve as a model for characterizing seismic source parameters in other understudied seismicity regions globally.

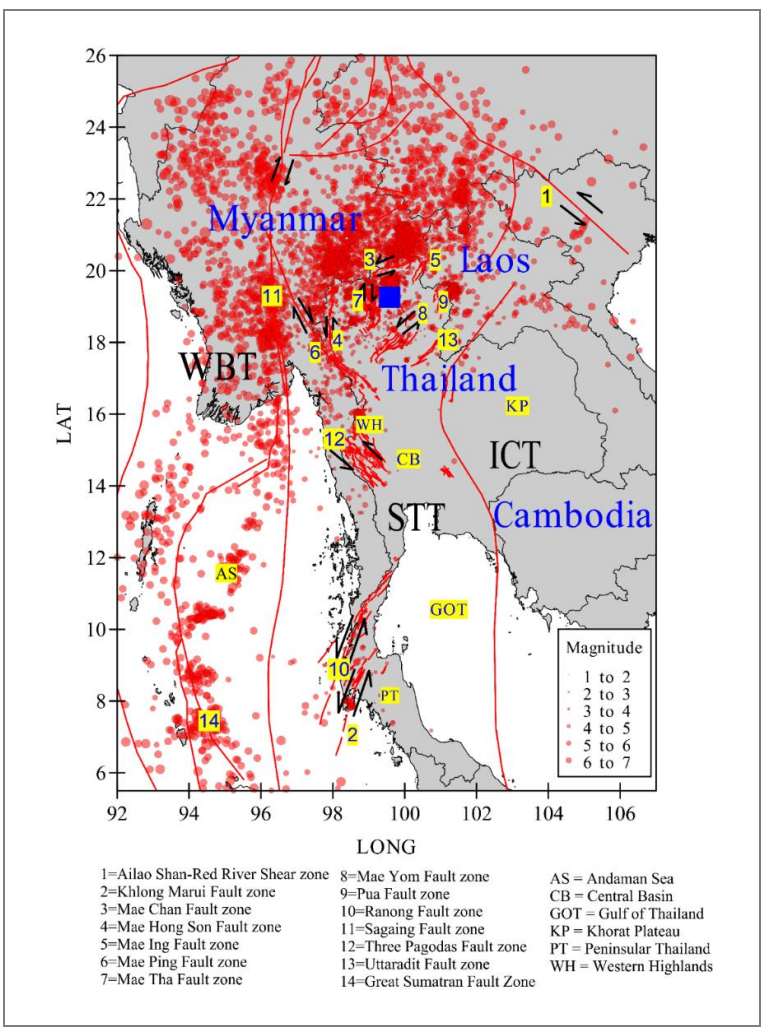

Figure 1 General tectonic setting of Thailand and its surrounding areas. Red circles indicate 9,792 seismic events reported by the Thai Meteorological Department (TMD) from 2009 to 2022. Red lines represent surface fault lines, as identified by Department of Mineral Resources (DMR) (2007) and Morley *et al*. (2011). Blue square highlights the study area. WBT: West Burma (Myanmar) Terrane, ICT: Indochina Terrane, STT: Shan-Thai Terrane.

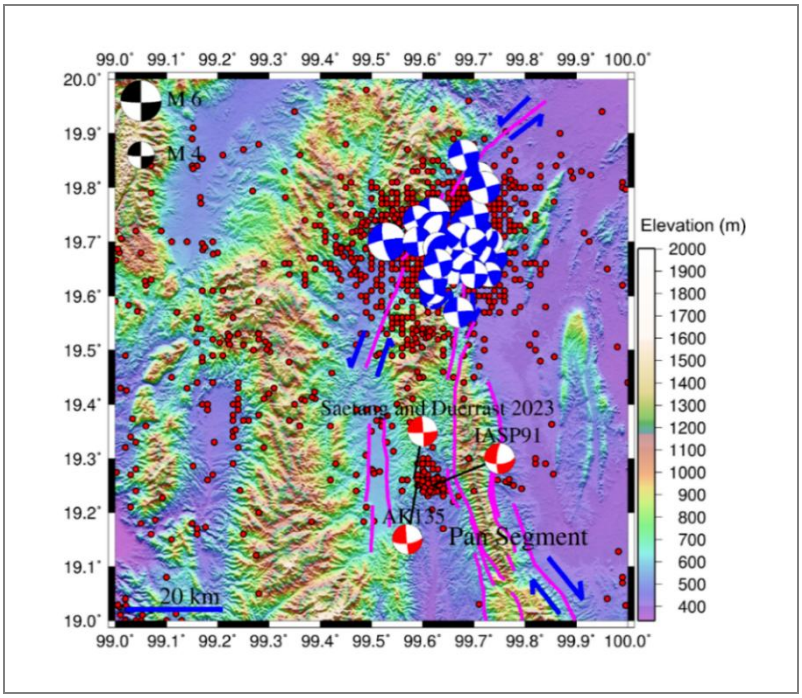

Figure 2 Phayao Fault Zone and focal mechanisms. Pink lines show fault segments. Red dots indicate earthquake epicenters from TMD (2009-2022). Red beach balls at Pan Segment represent focal mechanisms based on velocity models used in our analysis. Blue beach balls at Mae Lao Segment are from Pananont *et al.* (2017).

Research methods

For this study, we utilized seismic stations from four distinct networks, as depicted in Figure 3. These networks include the Global Seismograph Network (IU), the Myanmar National Seismic Network (MM), the Regional Integrated Multi-Hazard Early Warning System (RM), and the Thai Seismic Monitoring Network (TM). The integration of data from these multiple networks enhances the reliability and accuracy of the results. For the initial hypocenter determination, seven stations located within 200 km of the epicenter were selected, as this distance criterion ensured clear P- and S-wave first arrivals for accurate phase picking. For the waveform inversion, 10 stations from the four networks were utilized: SUAB, LAMP, CHTO, HOTB, KTN, NONG, TGI, YGN, SLV, and NGU (Figure 3). The inclusion of additional, more distant stations in the waveform inversion enhanced the azimuthal coverage and provided better constraints on the moment tensor solution. Data were downloaded through the Incorporated Research Institutions for Seismology (IRIS) platform, whereas the Thai Meteorological Department (TMD) provided direct access to TM data.

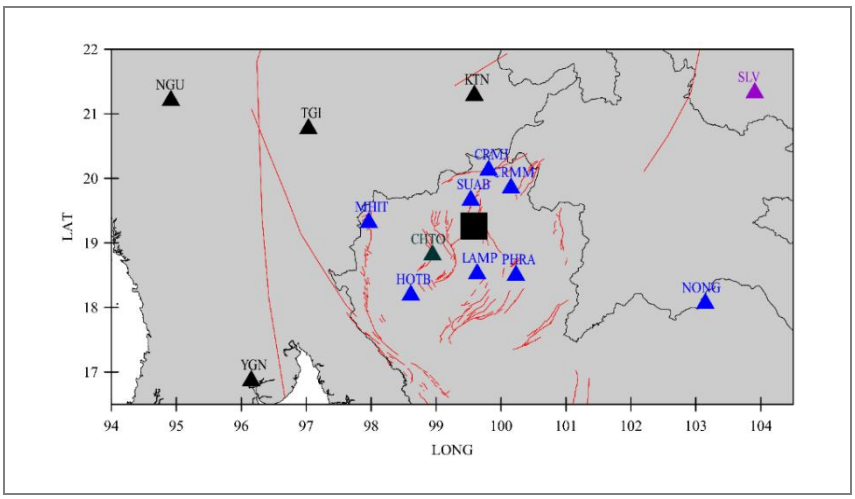

Figure 3 Distribution of seismic stations from four networks. Blue, green, black, and purple triangles illustrate stations from the TM, IU, MM, and RM networks, respectively. A black square indicates the study area. Red lines show fault lines.

Source: Department of Mineral Resources (DMR) (2007); Morley *et al*. (2011)

Identification of hypocentres, representing earthquake locations, was manually conducted by selecting initial P- and S-arrival times. Multiple velocity models were used in this process, including AK 135 (Kennett *et al*., 1995), IASP91 (Kennett and Engdahl, 1991), and a minimum 1-D velocity model with station delays from Saetang and Duerrast (2023). A modified version of the HYPOCENTER software (Lienert *et al*., 1986; Lienert and Havskov, 1995) with an earthquake location method that utilizes centered, scaled, and adaptively damped least squares, was used for hypocentral calculation, as incorporated by Seisan (Havskov and Ottemöller, 1999). Latitudes and longitudes obtained from HYPOCENTER were used and remained constant, whereas depths were systematically adjusted within the range of 0.5 to 35 km with increments of 0.5 km each, during the waveform inversion process.

In this research, we employed the ISOLA Fortran code (Sokos and Zahradník, 2008) for focal mechanism analyses. This freely available software is based on the six-element moment tensor approach proposed by Kikuchi and Kanamori (1991) and the inverse problem formulations developed by Zahradník and Plešinger (2005). Within this software, we utilized a single-point source solution and the deviatoric moment tensor (DMT) inversion technique. This technique requires two key components; a double-couple (DC), and a compensated linear vector dipole (CLVD), both with 0% volumetric coverage.

Due to the large-scale regions of hypocentral distances from stations, an automatic calculation of station weights was applied in the analysis using the ISOLA Fortran code (Sokos and Zahradník, 2008). For the estimation of centroid depths, a 3D spatial grid search methodology was employed, and the Green's function was computed using a frequency-wavenumber method (Bouchon, 1981). The Green's function was calculated using the AK135, IASP91, and a specific 1D velocity model (Saetang and Duerrast, 2023) with a maximum frequency limit of 0.10 Hz. This frequency band (0.03-0.10 Hz) was selected because surface waves, which dominate seismograms at regional distances, carry the most information for moment tensor inversion in this frequency range. Furthermore, we determined the densities of the crustal layers using equation (1),

$$\text{Density (g/cm}^3\text{)} = 1.7 + 0.2 \times V_p \text{ (km/s)} \quad (1)$$

The data processing procedures employed in this study involved several steps to ensure accuracy and reliability of the results. Before initiating the inversion process for the DMT analysis, it was necessary to apply instrumental corrections. These corrections consisted of removing the direct current (DC) offset and long-term trends from the observed waveforms. To prepare the waveforms for subsequent analysis, both the synthetic and observed data were band-pass filtered. The selected frequency range for the filtering process was set between 0.03 Hz and 0.10 Hz. Frequencies below 0.03 Hz were not expected to contribute significantly due to the presence of long-period noise and the inherent frequency limitations of the seismometers used in this study. Conversely, frequencies above 0.10 Hz were previously tested and found to yield inconsistent results compared to the observed waveforms. This inconsistency may be attributed to the hypocentral distances, which were not adequately small. A more detailed investigation and expansion of the selected frequency ranges have been carried out, as discussed in the subsequent sections of the study, specifically in the results and discussion.

Following the band-pass filtering and instrument corrections, the seismic data were converted from count units to displacement units, expressed in meters. This conversion was crucial for ensuring the data's physical meaningfulness and interpretability. Subsequently, the corrected data were truncated to encompass a time span of 250 seconds, starting from the hypocentral time. This duration was carefully selected to encompass all earthquake events under investigation, enabling a comprehensive analysis of the seismic signals. To improve analysis and computational efficiency, the data were automatically resampled from the original frequency to 33 Hz. This ensured temporal resolution while reducing the computational load on high-frequency components. By rigorously processing the data through instrument corrections, band-

pass filtering, unit conversion, truncation, and resampling, the seismic data were effectively prepared for detailed analysis, enabling an investigation into the seismic characteristics and properties of the studied earthquakes.

The DMT inversion process played a pivotal role in this study, aiming to minimize the discrepancies between observed and synthetic data in terms of displacements. By adopting a least-squares approach, the inversion considered trial origin times and trial source positions meticulously. The primary objective was to identify the optimal depth and time that would best align the observed and synthetic data. This search for the optimum parameters was conducted by incrementally exploring predefined intervals. For depth determination, a systematic exploration was carried out by incrementing the depth values according to a parameter derived from the Green's function. Each increment provided an opportunity to evaluate how well the synthetic data matched the observed data at different depths.

For time determination, a range of time steps was examined, each corresponding to 0.2 seconds. This time range extended from 5.0 seconds before the hypocentral time calculated from HYPOCENTER to 5.0 seconds after it. The resulting optimum depth and optimum time, obtained through this exhaustive search process, were referred to as the centroid depth and centroid time, respectively. These parameters represented the best-fit values that minimized the discrepancies between the observed and synthetic data. The determination of the centroid depth and centroid time provided crucial insights into the seismic source characteristics and temporal evolution of the studied earthquakes.

The determination of the best centroid positions (epicenters and depths) and time, based on the correlation coefficient between the observed and synthetic waveforms, is achieved through a grid-search method. The correlation coefficient represents the match between the waveforms and is quantified by a variance reduction. The variance reduction (var.red.) is calculated using the following equation (2),

$$\text{var.red} = 1 - \frac{E}{O} \tag{2}$$

where $E = \sum\left(O_i - S_i\right)^2$, $O = \sum O_i^2$, S is synthesis, and O is original waveforms along with the summation of all collected data. A higher value of var.red. indicates a better fit between observed and synthesised waveforms.

Waveform inversion is an important technique used in focal mechanism studies to determine seismic source parameters, such as strike, dip, and rake angles. The inversion tries to minimize differences between observed and synthetic waveforms, providing valuable insights into faulting mechanisms. The process finds model parameters that best

match the observed data, including arrival times, amplitudes, and waveform shapes. Here, three-component waveform inversions were performed using an iterative deconvolution method (Kikuchi and Kanamori, 1991). A waveform inversion approach was adopted without separating body and surface waves. The waveform fit was optimized through a grid search over various trial positions. The grid-search method employed and determined the best centroid positions and time based on the correlation coefficient, aiming to fit between the observed and synthetic waveforms.

Results and discussion

The Waveform inversion with multiple velocity models was selected to determine the focal mechanisms of earthquakes in the Pan Segment of the Phayao Fault Zone in Northern Thailand. Table 1 presents the calculated hypocenter parameters, including latitude, longitude, depth, and time of origin. Seven stations (CRMJ, CRMM, HOTB, LAMP, MHIT, PHRA, and SUAB) as illustrated in Figure 3. Each station was selected based on its hypocentral distance, ensuring that each station was situated within 200 km distance from the seismic events to ensure that arrival times could be determined from clear first breaks and arrivals, thus providing reliable and unambiguous data for waveform inversion analysis. The 200 km epicentral distance criterion was applied to ensure sufficient signal-to-noise ratio, and all available stations within this distance range were utilized. These stations provide azimuthal coverage from multiple directions relative to the epicenter (Figure 3). A seismic velocity model is essential to know for a region of interest, as it directly affects the accuracy of hypocentral determination. By comparing results obtained from multiple velocity models, a more comprehensive analysis and assessment of the uncertainties associated with hypocenter determination can be achieved.

The TMD (Thailand Meteorological Department) reported a seismic event in the Pan Segment of the Phayao Fault Zone that occurred on February 20, 2019, at 09:05:41 local time (UTC+07:00). The Saetang and Duerrast (2023) velocity model estimated the hypocenter at approximately 19.262° N and 99.583° E with a depth of 27.1 km. The AK135 model estimated the hypocenter at approximately 19.258° N and 99.590° E with a depth of 20.3 km. Further, the IASP91 model determined the hypocenter to be approximately 19.250° N and 99.620° E with a depth of 15.8 km.

To identify the most accurate velocity model for calculating hypocentral parameters within the Pan Segment, we conducted a comparative analysis. This involved evaluating various hypocentre results, which included the following parameters: latitude (LT), longitude (LN), depth (DP), and origin time. Additionally, we considered the error estimates (ER) for each parameter (ERLT, ERLN, and ERDP) as presented in Table 1.

Notably, the AK135 model exhibited a significantly higher error in depth (ERDP) at 46.6 km, suggesting less reliability in depth estimation compared to the Saetang and Duerrast (2023), and IASP91 models. Conversely, the IASP91 model yielded the lowest error estimates across all parameters, suggesting a potentially more reliable model for this specific region. Despite these observations, no single model emerged as the best for all parameters. Therefore, the determination of focal mechanisms for earthquakes within the Pan Segment, as presented in Table 2, required a careful discussion. This was particularly informed by waveform inversion results using various velocity models, whilst the error estimates from Table 1 provided additional context on the reliability and limitations of each model.

To summarize the results of the DMT inversion process using multiple velocity models, Table 2 presents an overview of the centroid depths and times for the analyzed earthquakes. The relatively low variance reduction values (0.13 to 0.37) are likely attributed to the limitations of 1-D velocity models in capturing three-dimensional crustal heterogeneities in this tectonically complex region, as well as the signal-to-noise ratio at the recording stations. This table includes event-specific details, such as velocity models, date and centroid time, latitude and longitude, centroid depth, moment magnitude (M_w), strike, dip, and rake angles for two nodal planes, double couple percentage (DC%), and variance reduction (var.red.).

Applying the Saetang and Duerrast (2023) velocity model, the centroid coordinates were estimated at 19.262° N and 99.583° E with a centroid depth of 8 km. The moment magnitude was calculated as M_w 4.4. The strike, dip, and rake angles for the first nodal plane were determined as 356°, 87°, and 173°, respectively, while the second nodal plane exhibited strike, dip, and rake angles of 087°, 83°, and 003°, respectively. The dip direction of the first nodal plane is 086° (eastward), which is consistent with the structural geology of the western Phayao Fault Zone characterized as a half-graben with an eastward dip direction. The DC% was determined to be 93.1, indicating a dominant doublecouple component, and the variance reduction was 0.13. Using the AK135 velocity model, the centroid coordinates were estimated at approximately 19.258° N and 99.590° E with a centroid depth of 6.5 km. The moment magnitude remained unchanged at M_w 4.4. The strike, dip, and rake angles for the first nodal plane were determined as 175°, 86°, and -158°, respectively, while the second nodal plane exhibited strike, dip, and rake angles of 084°, 68°, and -005°, respectively. The DC% was calculated as 61.2, and the variance reduction was 0.18. Using the IASP91 velocity model, the centroid was determined to be approximately 19.250° N and 99.620° E, with a centroid depth of 5.5 km. The moment magnitude was slightly higher with M_w 4.5. The strike, dip, and rake angles for the first nodal plane were computed as 184°, 75°, and -149°, respectively,

while the second nodal plane demonstrated strike, dip, and rake angles of 086°, 61°, and -017°, respectively. The DC% was evaluated as 50.7, and the variance reduction was 0.37.

As waveform inversion is used to determine the focal mechanisms of earthquakes in the Pan Segment of the Phayao Fault Zone, variance reduction serves as a key metric for evaluating the reliability of the results. A higher value of variance reduction suggests a better fit between observed and synthetic waveforms. This, in turn, increases confidence in the derived focal mechanisms. We used variance reduction as a quantitative measure to assess this fit. The IASP91 velocity model yielded the highest variance reduction, with a value of 0.37. It was followed by the AK135 model with 0.18 and the Saetang and Duerrast (2023) model with 0.13. Results are detailed in Table 2. A visual representation of the fit between observed and synthetic waveforms is shown in Figure 4. However, it is essential to note that variance reduction is not the only criterion for model selection. For a more nuanced understanding of the correlation between each model and seismic data across parameters such as time shift, depth, and focal mechanism, readers are referred to Figure 5, 6, and 7.

Table 1 Hypocenters determined by the HYPOCENTER computer program using multiple velocity models.

Velocity model	Date (DD/MM/YYYY)	Local time (UTC+07:00)	Latitude (° N)	Longitude (° E)	Depth (km)	RMS (s)	ERLN (km)	ERLT (km)	ERDP (km)
Saetang and Duerrast, 2023	20/02/2019	09:05:39.49	19.262	99.583	27.1	0.38	2.5	1.2	6.6
AK135	20/02/2019	09:05:41.17	19.258	99.590	20.3	0.59	4.5	2.0	46.6
IASP91	20/02/2019	09:05:40.87	19.250	99.620	15.8	0.30	2.2	0.9	2.4

Note: - RMS = root mean square; ERLN = longitude error; ERLT = latitude error; and ERDP = depth error.

Table 2 Results from the DMT inversion using multiple velocity models are illustrated in Figure 4.

Velocity model	Date (DD/MM/YYYY)	Centroid time (UTC+07:00)	Latitude (° N)	Longitude (° E)	Centroid Depth (km)	M_w	Strike1	Dip1	Rake1	Strike2	Dip2	Rake2	DC%	Var.red.
Saetang and Duerrast, 2023	20/02/2019	09:05:39.73	19.262	99.583	8	4.4	356	87	173 right	87	83	3	93.1	0.13
AK135	20/02/2019	09:05:44.11	19.258	99.590	6.5	4.4	175	86	-158 right	84	68	-5	61.2	0.18
IASP91	20/02/2019	09:05:41.11	19.250	99.620	5.5	4.5	184	75	-149 right	86	61	-17	50.7	0.37

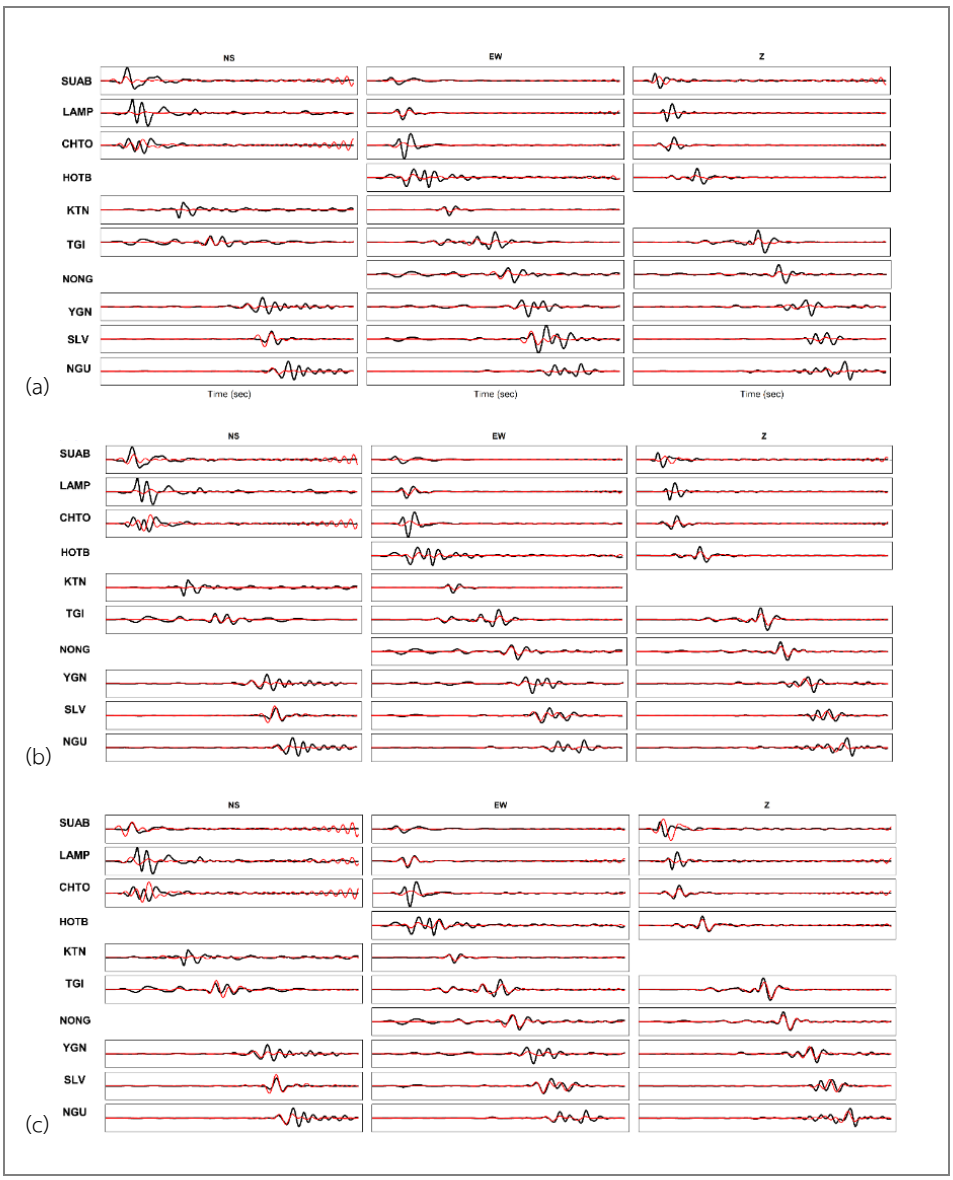

Figure 4 Comparative analysis of waveform inversions using multiple velocity models: the Saetang and Duerrast (2023) velocity model (a), the AK135 model (b), and the IASP91 model (c).

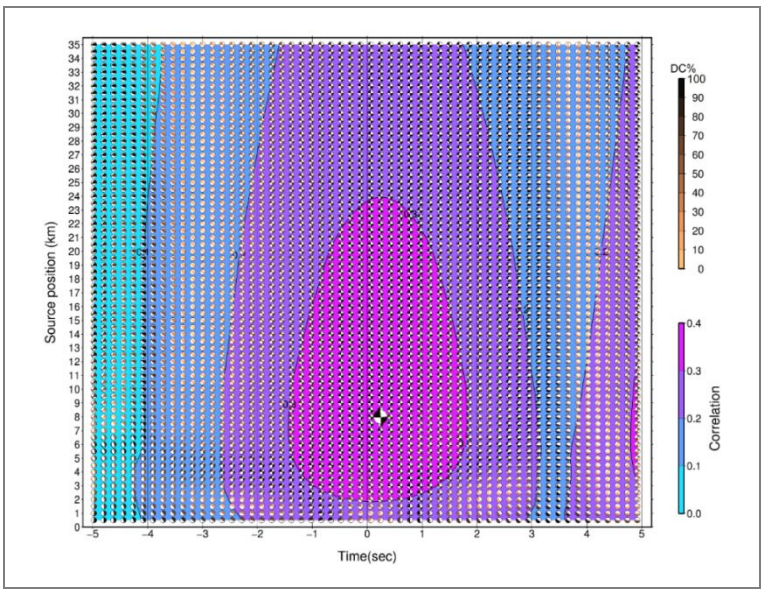

Figure 5 Correlation versus time shift and depths for single-source inversion. Using the Saetang and Duerrast (2023) model. Higher correlation values indicate a more accurate fit between seismic data and model parameters, such as time shift and depth.

Source: Sokos and Zahradník (2008)

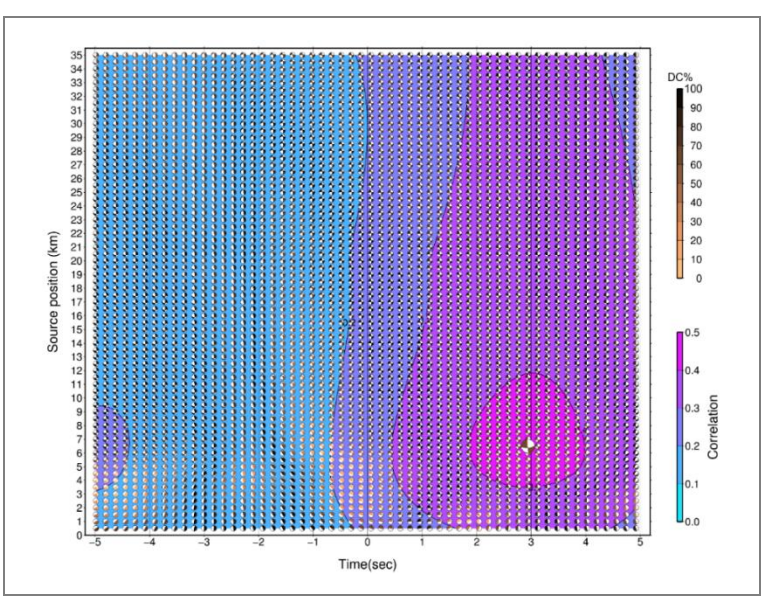

Figure 6 Correlation versus time shift and depths for single-source inversion using the AK135 model. Higher correlation values indicate a more accurate fit between seismic data and model parameters, such as time shift and depth.

Source: Sokos and Zahradník (2008)

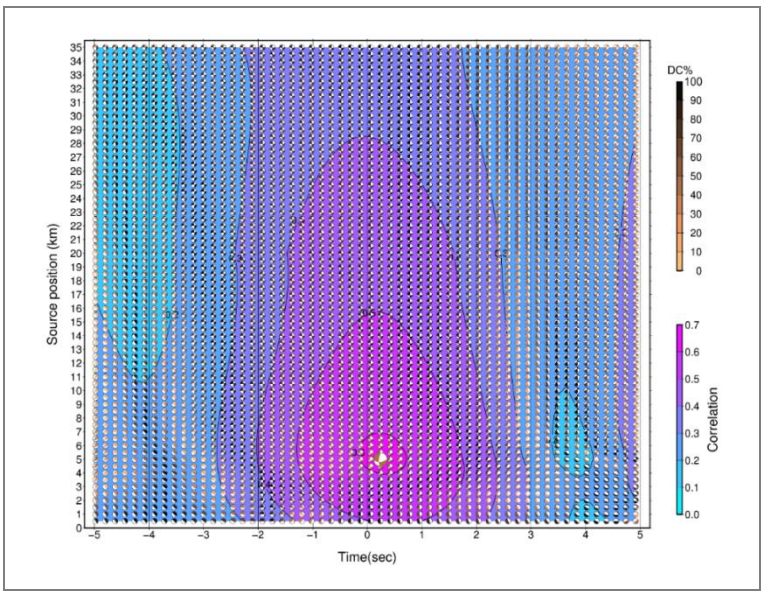

Figure 7 Focal mechanism for single-source inversion using the IASP91 model. Higher correlation values indicate a more accurate fit between seismic data and model parameters, such as focal mechanism.

Source: Sokos and Zahradník (2008)

Interestingly, the high variance reduction value for the IASP91 model aligns well with the geological features of the Pan Segment. This highlights the importance of integrating seismological and geological data for a more complete understanding of earthquake mechanisms. Geological consistency and double-couple percentages also play a significant role. For instance, the Saetang and Duerrast (2023) model has a relatively high DC% value of 93.1. While variance reduction is an important metric, not the sole criterion for model selection, these values come with limitations. A high value does not necessarily imply that the model is free from errors or uncertainties. Future studies could focus on a more in-depth uncertainty analysis to validate the robustness of the waveform inversion results. To determine the most suitable model for the Pan Segment region, it is essential to consider not only the variance reduction but also additional geological information, such as fault strike from geological maps.

Strike angles from the first nodal plane, obtained from all velocity models, consistently align with the fault line depicted in Figure 2, showing a clear north-south trending pattern. The strike angles from the second nodal plane across all velocity models do not exhibit a discernible relationship with geological or topographic maps. By comparing results obtained from multiple velocity models, the fault orientations illustrated in Figure 2 are considered. Fault orientations of the Pan Segment follow

approximately a north-south trend, where the strike angle is assumed to be a value between 0 and 180 degrees. This emphasises again that integrating geological and seismological data into earthquake studies is essential, especially for identifying the correct nodal plane. Based on these findings, we interpreted and considered only the strike angles from the first nodal plane for determining the rake angle.

The rake angle characterizes the direction of movement of the hanging wall during fault rupture relative to the fault strike (-180 to 180 degrees). A rake angle of 0 degrees indicates left-lateral motion; while +/-180 degrees signify right-lateral motion. Positive rake angles involve upward movement (thrust/reverse fault), while negative angles indicate downward movement (normal fault) (Aki and Richards, 1980). Based on the focal mechanisms derived from the results presented in Table 2, it is evident that the earthquakes occurring in the Pan Segment of the Phayao Fault Zone in Northern Thailand predominantly exhibit right-lateral strike-slip motion. This conclusion is drawn from the consistent rake angles provided in the table for the first nodal planes across the three velocity models. In each case, the obtained rake angles are close to +/-180 degrees, confirming the predominant right-lateral strike-slip characteristic.

The double couple percentage (DC%) is an important parameter to assess the generality of pure shear motion during seismic events. A higher DC% indicates a dominant presence of strike-slip or dip-slip faulting, while a lower value suggests the involvement of non-pure shear components. Notably, the recent model presented by Saetang and Duerrast (2023) reveals a significantly higher DC% values of 93.1, contrasting with lower DC% values found in the other two velocity models, namely 61.2 for AK135, and 50.7 for IASP91. A complex rupture and normal faulting earthquake system may lead to lower DC% values (Zaccagnino and Doglioni, 2022). However, this explanation might not hold for the lower DC% values observed in AK135 and IASP91 compared to the model of Saetang and Duerrast (2023), as the same event within the same fault zone should yield similar DC% levels. Instead, Zahradník and Sokos (2018) propose that a low DC% might indicate an issue with the velocity model. Consequently, it can be inferred that the velocity model published by Saetang and Duerrast (2023), based on localearthquake travel-time data in Northern Thailand, is better suited for focal mechanism analyses in the Pan Segment. Hence, the determination of the strike, dip, and rake angles for the first nodal plane of the event that occurred on 20 February 2019, in the Pan Segment of the Phayao Fault Zone with values of 356°, 87°, and 173°, respectively, is considered reasonable and very likely.

The local velocity model (Saetang and Duerrast, 2023) yielded the highest double-couple percentage. This result is consistent with the understanding that non-double-couple components can arise as artifacts when the velocity model does not

accurately represent the Earth's structure. The local model, derived from earthquake data in Northern Thailand, better captures regional crustal characteristics, resulting in more accurate Green's functions and focal mechanisms with higher double-couple components.

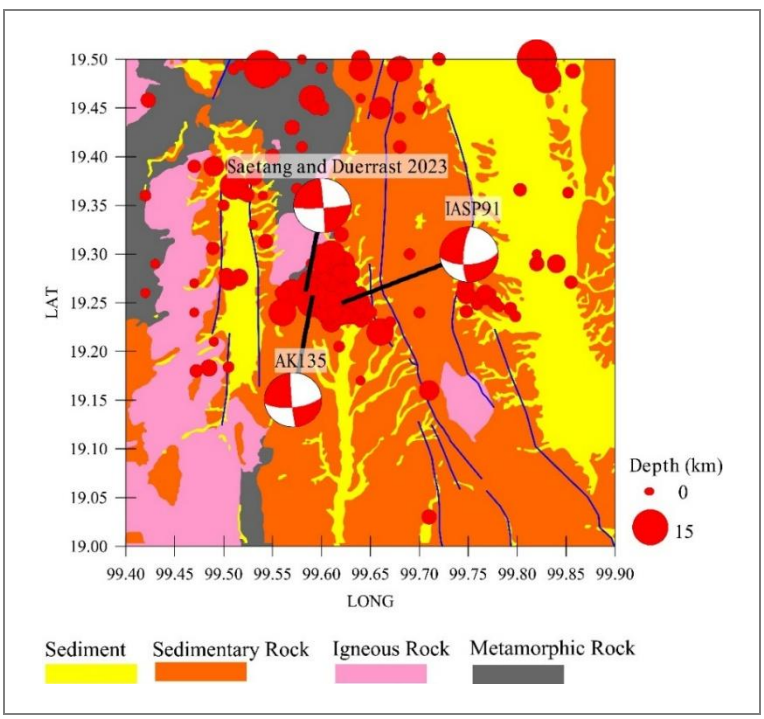

Figure 8 Hypocenter locations and focal mechanisms of the February 20, 2019 earthquake sequence in the Pan Segment of the Phayao Fault Zone, Northern Thailand. Locations were determined using the Saetang and Duerrast (2023), AK135, and IASP91 models. Seismic events from the TMD catalog (2009–2022) are denoted by circles, with circle diameter scaled proportionally to hypocenter depth (larger circles indicate deeper events; see legend inset). Beach ball diagrams represent the faulting mechanisms derived for each velocity model. The color-coded background illustrates the regional geological framework, comprising sedimentary, igneous, and metamorphic lithological units.

Figure 8 presents a comprehensive synthesis of the hypocenter locations and focal mechanisms derived for the 20 February 2019 earthquake sequence in the Pan Segment of the Phayao Fault Zone, Northern Thailand. Red circles indicate events reported by the Thai Meteorological Department (TMD), with the size of each circle proportional to the hypocenter depth. This depth-dependent scaling provides a clear

visualization of the spatial distribution and depth variation of the seismic events. Notably, the highest seismicity area, as indicated by the concentration of red circles, coincides with the epicentral locations determined by the Saetang and Duerrast (2023), AK135 (Kennett *et al*., 1995), and IASP91 (Kennett and Engdahl, 1991) velocity models for the February 20, 2019 earthquake. This convergence of seismicity and the epicentral locations derived from multiple velocity models underscores the significance of this area as a focal point of seismic activity within the Pan Segment.

The focal mechanisms, represented by beach ball diagrams, illustrate the predominance of strike-slip faulting mechanisms derived from each velocity model. The consistency of these mechanisms across different models offers crucial insights into the orientation and sense of motion of the fault planes responsible for the earthquakes, reinforcing the reliability of the derived fault plane solutions. The strike-slip mechanisms indicate lateral motion along the fault, suggesting a dominant role of shear stress in the tectonic setting of the Pan Segment.

The color-coded background of Figure 8 represents the regional geological framework, encompassing sedimentary, igneous, and metamorphic lithological units. The integration of geological context with seismological data enables a comprehensive understanding of the relationships among earthquake locations, fault mechanisms, and the underlying lithology. The spatial distribution of the hypocenters reveals a clustering of seismic events within the Pan Segment, particularly in the area of highest seismicity, indicating the active nature of this fault zone. The depth distribution of the hypocenters, as evidenced by the varying sizes of the red circles, suggests that the earthquakes occurred at different depths within the crust, which may be attributed to the complex interplay of tectonic stresses and the presence of multiple fault segments or splays within the Pan Segment (Boonchaisuk *et al*., 2017; Department of Mineral Resources (DMR), 2007).

The integration of the geological framework in Figure 8 enables a more comprehensive interpretation of seismicity in the Pan Segment. The presence of different lithological units, such as sedimentary, igneous, and metamorphic rocks, may influence the propagation of seismic waves and the distribution of crustal stress (Saetang *et al*., 2017; Saetang and Duerrast, 2023). The alignment of the hypocenters with specific geological features, such as fault boundaries or lithological contacts, can provide insights into the structural controls on the earthquake locations and mechanisms.

Figure 8 provides a detailed and integrated analysis of the hypocenter locations and focal mechanisms of the 20 February 2019 earthquake sequence in the Pan Segment of the Phayao Fault Zone. The coincidence of the highest seismicity area with the epicentral locations determined by multiple velocity models underscores the

robustness of the seismological analysis. It highlights the significance of this area in understanding the tectonic setting and seismic hazard of the region. The predominance of strike-slip faulting mechanisms derived from different velocity models reinforces the reliability of the fault plane solutions. It provides a consistent picture of the tectonic regime in the Pan Segment. The combination of seismological data and geological context provides a comprehensive framework for unravelling the complex nature of the fault zone and the potential influence of lithological heterogeneity on the seismicity. This integrated approach serves as a valuable tool for seismic hazard assessment and further research in the Pan Segment and similar tectonic environments.

Conclusion

In this study, we have gained invaluable insights into the focal mechanisms of the Pan Segment of the Phayao Fault Zone in Northern Thailand. Utilizing waveform inversion techniques, we employed multiple velocity models, including Saetang and Duerrast (2023), AK135, and IASP91, to analyses seismic data from four different networks. Our comprehensive analysis revealed a complex interplay of strike-slip and reverse faulting, with a dominant mechanism of right-lateral strike-slip faulting. This finding is particularly significant for seismic hazard assessment in the region. The study also highlighted the importance of variance reduction in validating the reliability of our models. Furthermore, the results presented here are consistent with the fault geometry and orientation of the Pan Segment. Among the models used, the Saetang and Duerrast (2023) model yielded the highest double-couple percentage (DC%), suggesting its potential accuracy for calculating hypocentral parameters in this specific context. This is the first study to employ the Saetang and Duerrast (2023) model for this particular geological setting, offering a new benchmark for future research. Our findings also introduce a novel perspective on the interplay among faulting mechanisms, which has not been reported previously for the Pan Segment. Specifically, the coexistence of right-lateral strike-slip and reverse faulting components indicates that the Pan Segment is subjected to a transpressional stress regime, wherein both horizontal shear and compressional stresses are simultaneously active across the fault zone. These advancements have critical implications for seismic hazard assessment and model validation, setting the stage for future research not only in this area but also in other similar regions worldwide. Further, the findings underscore the need for additional research to fine-tune the models and methodologies used here.

Acknowledgements

The authors extend their sincere gratitude to the Thailand Meteorological Department (TMD) and the Incorporated Research Institutions for Seismology (IRIS) for providing seismic data. Special thanks to Patinya Pornsopin for his outstanding technical support in the TM network, which greatly facilitated this study.

References

Aihara, K., Takemoto, K., Zaman, H., Inokuchi, H., Miura, D., Surinkum, A., Paiyarom, A., Phajuy, B., Chantraprasert, S., Panjasawatwong, Y., Wongpornchai, P. and Otofuji, Y. (2007). Internal deformation of the Shan-Thai block inferred from paleomagnetism of Jurassic sedimentary rocks in Northern Thailand. *Journal of Asian Earth Sciences,* 30(3-4), 530-541, doi: https://doi.org/10.1016/j.jseaes.2007.01.002.

Aki, K. and Richards, P.G. (1980). *Quantitative seismology: Theory and methods, volumes I and II*. San Francisco: W.H. Freeman and Co.

Boonchaisuk, S., Noisagool, S., Amatyakul, P., Rung-Arunwan, T., Vachiratienchai, C. and Siripunvaraporn, W. (2017). 3-D magnetotelluric imaging of the Phayao Fault Zone, Northern Thailand: Evidence for saline fluid in the source region of the 2014 Chiang Rai earthquake. *Journal of Asian Earth Sciences*, 147, 210-221, doi: https://doi.org/10.1016/j.jseaes.2017.07.034.

Bouchon, M. (1981). A simple method to calculate green's functions for elastic layered media. *Bulletin of the Seismological Society of America*, 71(4), 959-971, doi: https://doi.org/10.1785/BSSA0710040959.

Department of Mineral Resources (DMR). (2007). *Geological map of Thailand (scale 1:1,000,000)*. Bangkok: Department of Mineral Resources.

Havskov, J. and Ottemöller, L. (1999). SeisAn earthquake analysis software. *Seismological Research Letters*, 70(5), 532-534, doi: https://doi.org/10.1785/gssrl.70.5.532.

Kennett, B.L.N. and Engdahl, E.R. (1991). Traveltimes for global earthquake location and phase identification. *Geophysical Journal International*, 105(2), 429-465, doi: https://doi.org/10.1111/j.1365-246X.1991.tb06724.x.

Kennett, B.L.N., Engdahl, E.R. and Buland, R. (1995). Constraints on seismic velocities in the Earth from traveltimes. *Geophysical Journal International,* 122(1), 108-124, doi: https://doi.org/10.1111/j.1365-246X.1995.tb03540.x.

Kikuchi, M. and Kanamori, H. (1991). Inversion of complex body waves-III. *Bulletin of the Seismological Society of America*, 81(6), 2335-2350, doi: https://doi.org/10.1785/BSSA0810062335.

Lienert, B.R. and Havskov, J. (1995). A computer program for locating earthquakes both locally and globally. *Seismological Research Letters*, 66(5), 26-36, doi: https://doi.org/10.1785/gssrl.66.5.26.

Lienert, B.R., Berg, E. and Frazer, L.N. (1986). Hypocenter: An earthquake-location method using centered, scaled, and adaptively damped least squares. *Bulletin of the Seismological Society of America,* 76(3), 771-783, doi: https://doi.org/10.1785/BSSA0760030771.

Morley, C.K., Charusiri, P. and Watkinson, I.M. (2011). Structural geology of Thailand during the Cenozoic. In Ridd, M.F., Barber, A.J. and Crow, M.J. (Eds.). *The geology of Thailand*, pp. 273-334. London: Geological Society of London.

Noisagool, S., Boonchaisuk, S., Pornsopin, P. and Siripunvaraporn, W. (2014). Thailand's crustal properties from teleseismic receiver-function studies. *Tectonophysics,* 632, 64-75, doi: https://doi.org/10.1016/j.tecto.2014.06.014.

Pananont, P., Herman, M.W., Pornsopin, P., Furlong, K.P., Habangkaem, S., Waldhauser, F., Wongwai, W., Limpisawad, S., Warnitchai, P., Kosuwan, S. and Wechbunthung, B. (2017). Seismotectonics of the 2014 Chiang Rai, Thailand, earthquake sequence. *Journal of Geophysical Research: Solid Earth*, 122(8), 6367-6388, doi: https://doi.org/10.1002/2017JB014085.

Saetang, K. (2017). Focal mechanisms of Mw 6.3 aftershocks from waveform inversions, Phayao Fault Zone, Northern Thailand. *International Journal of Geophysics,* 2017, 9059825, doi: https://doi.org/10.1155/2017/9059825.

Saetang, K. (2022). Two-layer model of anisotropy beneath Myanmar and Thailand revealed by shear-wave splitting. *Annals of Geophysics*, 65(6), SE213, doi: https://doi.org/10.4401/ag-8769.

Saetang, K. and Duerrast, H. (2023). A minimum 1-D velocity model of Northern Thailand. *Journal of Seismology,* 27, 493-504, doi: https://doi.org/10.1007/s10950-023-10148-6.

Saetang, K., Srisawat, W. and Duerrast, H. (2018). Crustal structures, geothermal sources and pathways beneath Northern Thailand revealed by local earthquake tomography. *Chiang Mai Journal of Science*, 45(1), 565-575.

Sokos, E.N. and Zahradník, J. (2008). ISOLA a Fortran code and a MATLAB GUI to perform multiple-point-source inversion of seismic data. *Computers and Geosciences,* 34(8), 967-977, doi: https://doi.org/10.1016/j.cageo.2007.07.005.

Thai Meteorological Department (TMD). (2014). *Chiang Rai earthquake report, 5 May 2014 (18:08 LST)*. Retrieved 15 May 2014, from: https://earthquake.tmd.go.th/documents/file/seismo-doc-1404703458.pdf.

Uttamo, W. (2000). *Structural and sedimentological evolution of Tertiary sedimentary basins in Northern Thailand*. Ph.D. thesis in Geology. Royal Holloway, University of London, Egham.

Zaccagnino, D. and Doglioni, C. (2022). The impact of faulting complexity and type on earthquake rupture dynamics. *Communications Earth and Environment*, 3, 258, doi: https://doi.org/10.1038/s43247-022-00593-5.

Zahradník, J. and Plešinger, A. (2005). Long-period pulses in broadband records of near earthquakes. *Bulletin of the Seismological Society of America*, 95(5), 1928-1939, doi: https://doi.org/10.1785/0120040210.

Zahradník, J. and Sokos, E. (2018). ISOLA code for multiple-point-source modeling: Review. In D'Amico, S. (Ed.). *Moment tensor solutions: A useful tool for seismotectonics*, pp. 1-28. Berlin: Springer.